Title

Critical Role of Methylammonium Librational Motion in Methylammonium Lead Iodide (CH3NH3PbI3) Perovskite Photochemistry

Journal

Nano Letters, 17(7)

ISSN

1530-6984

Authors

Park, Myeongkee

Kornienko, Nikolay

Reyes-Lillo, Sebastian E

et al.

Publication Date

2017-07-12

DOI

10.1021/acs.nanolett.7b00919

Peer reviewed

NANO LETTERS

Letter

pubs.acs.org/NanoLett

Critical Role of Methylammonium Librational Motion in Methylammonium Lead Iodide ($CH_3NH_3PbI_3$) Perovskite Photochemistry

Myeongkee Park,[†] Nikolay Kornienko,[†] Sebastian E. Reyes-Lillo,[‡,§] Minliang Lai,[†] Jeffrey B. Neaton,[‡,§,∥] Peidong Yang,[†,∥,⊥] and Richard A. Mathies*[,†]

[†]Department of Chemistry, [§]Department of Physics, [⊥]Department of Materials Science and Engineering, University of California, Berkeley, California 94720, United States

[‡]Molecular Foundry, Lawrence Berkeley National Laboratory, Berkeley, California 94720, United States

[∥]Kavli Energy NanoSciences Institute at Berkeley, Berkeley, California 94720, United States

Supporting Information

ABSTRACT: Raman and photoluminescence (PL) spectroscopy are used to investigate dynamic structure−function relationships in methylammonium lead iodide ($MAPbI_3$) perovskite. The intensity of the 150 cm^{-1} methylammonium (MA) librational Raman mode is found to be correlated with PL intensities in microstructures of $MAPbI_3$. Because of the strong hydrogen bond between hydrogens in MA and iodine in the PbI_6 perovskite octahedra, the Raman activity of MA is very sensitive to structural distortions of the inorganic framework. The structural distortions directly influence PL intensities, which in turn have been correlated with microstructure quality. Our measurements, supported with first-principles calculations, indicate how excited-state MA librational displacements mechanistically control PL efficiency and lifetime in $MAPbI_3$—material parameters that are likely important for efficient photovoltaic devices.

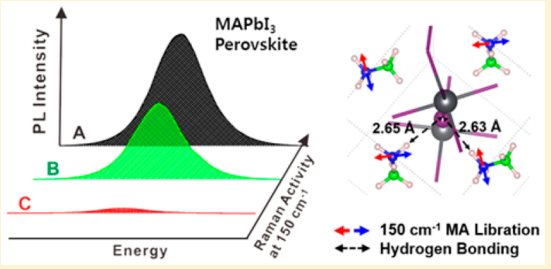

KEYWORDS: *Methylammonium lead iodide perovskite, $MAPbI_3$, photovoltaics, photoluminescence microscopy, Raman microscopy, DFT*

Recently there has been tremendous interest in photovoltaic (PV) materials containing methylammonium (CH_3NH_3, MA) lead iodide ($MAPbI_3$) perovskite because of its high and steadily improving quantum yield, PV efficiency, and its potential for low-cost fabrication.[1,2] $MAPbI_3$ materials have been studied extensively to gain insights regarding light absorption, charge separation, charge transport, and tolerance to crystallographic defects as well as how these factors play roles in overall device performance.[3−13] In particular, the role of MA has been examined in detail with the goal of understanding why $MAPbI_3$ is such a high-performing PV material.[14−17]

The properties of MA relevant for the function of $MAPbI_3$ include its size, position, orientation, and hydrogen-bonding (HB) flexibility in the inorganic Pb−I framework. In addition to providing a counterion for PbI_3^-, the size of the MA organic moiety is appropriate for an ideal "ABX_3" perovskite phase, and the structure of the inorganic Pb−I framework is highly sensitive to changes of MA position and orientation.[18−20] It was suggested that MA interacts with the Pb−I framework through HB between the ammonium hydrogens and the iodine atoms of the PbI_3^- cage, perturbing the conduction band minimum (CBM) and inducing a dynamical change of the band gap that increases the carrier diffusion length and suppresses electron−hole recombination.[21−23] In addition, the alignment of MA dipoles during polaron formation[24,25] and ferroelectric domain formation may play a role in the efficiency of $MAPbI_3$ materials.[26−30] In particular, recent theoretical studies have reported that an energy band splitting (Rashba splitting) can be induced by orientational changes of the MA dipoles that break the inversion symmetry of the spin−orbit activated $MAPbI_3$ system inducing an indirect band gap.[31] The longer excited-state lifetime associated with an indirect band gap material may make it easier for charge separation processes to compete with radiative and nonradiative recombination producing higher PV efficiency in a complete device.[32] In addition, MA groups also participate in the humidity related degradation of organic−inorganic hybrid perovskite PV materials, since water can hydrogen bond with the amine moiety.[33,34] This degradation leads to the exclusion of the MA^+ ions and eventually full degradation to the PbI_6^{4-} framework.[35−38] Thus, the interplay between the MA groups and the Pb−I octahedra may have several significant structural and functional consequences for $MAPbI_3$ perovskite, including charge-recombination dynamics, dielectric properties, and degradation pathways.

Received: March 3, 2017
Revised: May 8, 2017
Published: May 31, 2017

DOI: 10.1021/acs.nanolett.7b00919
Nano Lett. 2017, 17, 4151−4157

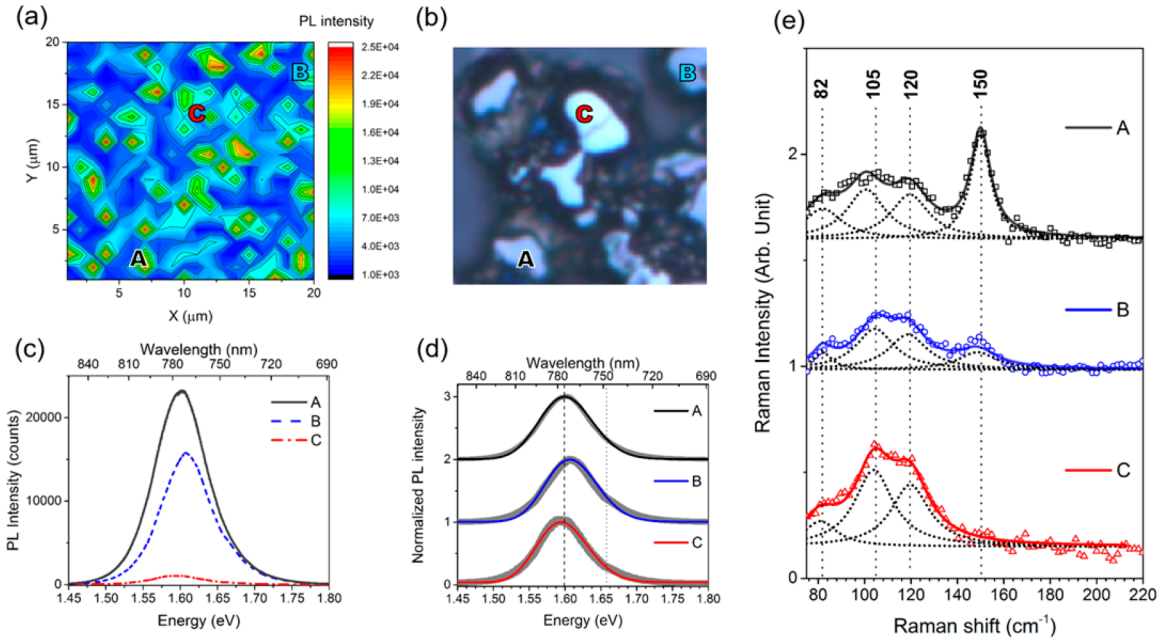

Figure 1. (a) Contour plot of PL intensity and (b) optical image of fresh $MAPbI_3$ film, (c) PL spectra measured at representative spots **A**, **B**, and **C**, (d) their normalized PL spectra, and (e) Raman spectra with fitting results using log-normal and Lorentzian spectral shape functions, respectively. Detailed fitting results are summarized in Tables S1 and S2.

Raman spectroscopy is a useful technique for selectively studying the vibrational structure and structural dynamics of MA in $MAPbI_3$ perovskite, complementing the static information available from techniques such as X-ray diffraction (XRD).[39,40] In previous Raman spectra of $MAPbI_3$, several low-frequency modes are observed below 300 cm^{-1}. These modes are composed of bending or stretching motions of the octahedral PbI_6^{4-} framework below 100 cm^{-1} and librational motions of MA at ~150 cm^{-1}.[6,41,42] Recent Raman studies reported prominent changes of MA Raman peak intensities in different perovskite structures induced by different crystal symmetries, crystallization on a mesoporous substrate, and intense light illumination.[43,44] These results indicate that the vibrational modes of MA are characteristic of, and unique to, these different $MAPbI_3$ structures. A correlated Raman signature was also reported in studies of charge-transfer efficiency in halide (X)-substituted $MAPbX_3$.[41] However, considering the potentially inhomogeneous nature of microstructures in $MAPbI_3$ films exhibiting different charge-recombination rates, macroscopically measured Raman spectra provide only limited spatially averaged information.[39,45]

It is necessary to carry out microscopic photoluminescence (PL) and Raman measurements on individual $MAPbI_3$ microstructures to go beyond the ensemble average. Such studies can reveal the mechanistic role of organic MA groups in determining optoelectronic properties and degradation pathways. Herein, we present (1) macroscopic PL measurements on fresh and degraded $MAPbI_3$ and (2) microscopic PL and Raman measurements from multiple microspots on $MAPbI_3$ films. Correlations are found between PL intensities and the observation of MA specific Raman peaks, suggesting that the intense librational motion of MA at 150 cm^{-1} is diagnostic of the high PL intensity, which has been found to correlate with PV device functionality.[8,11] First-principles density functional theory (DFT) calculations are performed to obtain further insight into the vibrational properties of the room temperature tetragonal structure of $MAPbI_3$ and to qualitatively describe the interactions between MA and the Pb−I framework. Our results suggest that the librational motion of MA induces a structural distortion of the framework resulting in a longer excited-state lifetime. Thus, this MA libration may play a significant role in the high PL efficiency/longer excited-state lifetime and potentially the overall efficiency of perovskite PV cells.

A $MAPbI_3$ perovskite film was prepared by the solvent method (see Supporting Information). Figure S1 presents the macroscopic absorbance and normalized PL spectrum excited with 532 nm excitation. These samples feature a uniformly high optical density (OD) from the visible to the near-infrared and an emission maximum at 777 nm (1.596 eV), while PbI_2 absorbance is only apparent below 520 nm.[46,47] The sample has no measurable PbI_2 reflections in the XRD spectrum (Figure S2).

PL microscopy was employed on several microspots to study the microheterogeneity of $MAPbI_3$ polycrystalline film.[48] Figure 1a and b presents a PL contour map image which has discrete PL intensities at numerous sites compared to an optical image of the sample, respectively. Figure 1c shows representative PL spectra of three different microspots with different intensities and different peak center wavelengths: spot **A** has the highest PL intensity; spot **B** shows the second brightest PL, and its intensity is approximately two-thirds that of **A** with a small blue-shift; spot **C** shows much weaker PL clearly distinguishable from the others.

The PL spectra were fit to log-normal line shape functions and plotted in Figure 1d. The fitting results are summarized in Table S1. The brightest PL peak in spot **A** is centered at 1.598 eV (776.0 nm). The other PL peaks from site **B** and **C** are located at 1.607 eV (772.1 nm) and 1.595 eV (777.4 nm), respectively. These results are consistent with the macroscopically measured PL peak center of the sample in Figure S1, but the full-width at half-maximum (fwhm) of spot **A** is 0.090 eV, narrower than the 0.103 eV found in the macroscopic measurements shown in Table S1. In addition, the PL spectra of spots **B** and **C** are even narrower, 0.088 and 0.082 eV fwhm,

DOI: 10.1021/acs.nanolett.7b00919
Nano Lett. 2017, 17, 4151−4157

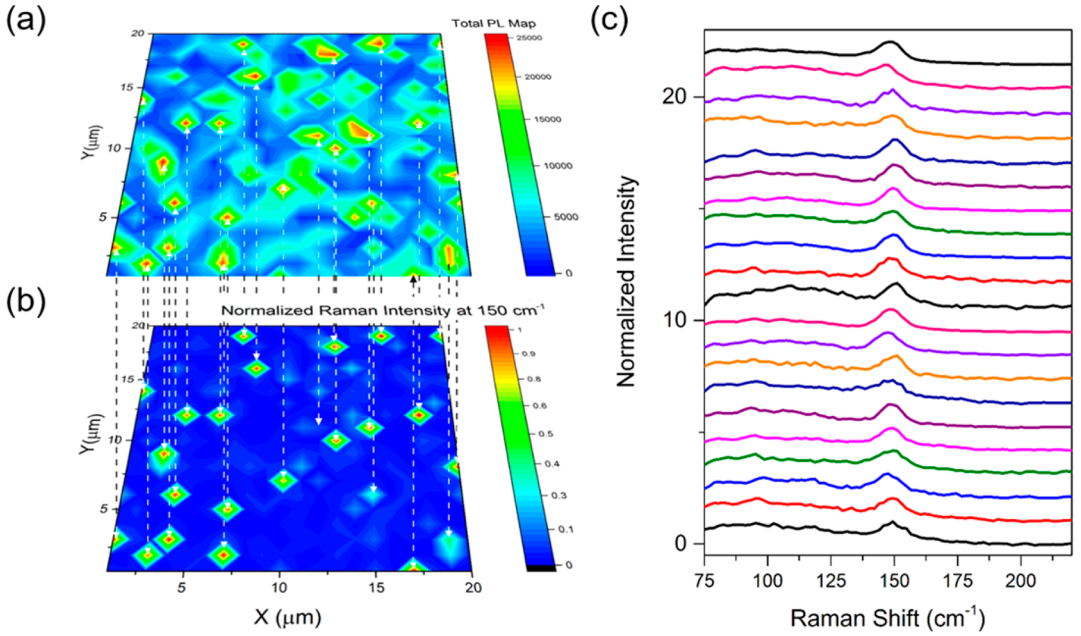

Figure 2. Contour plots of (a) PL intensities and (b) normalized Raman intensities measured at 150 cm^{-1}. (c) Normalized Raman spectra measured at the higher PL intensity (greater than 22 000 PL counts) spots from panel b.

respectively. The different widths clearly indicate that the macroscopically measured PL spectrum is composed of several narrower PL peaks from spatially inhomogeneous microstructures in a polycrystalline film. However, considering that these microscopically measured PL peak centers are not significantly different, we can speculate that the different PL intensities of spots **A**–**C** are mostly governed by quenching effects, consistent with the recent time-resolved PL result of deQuilettes et al.[45] Thus, the brightest spot **A** likely has fewer nonradiative channels with fewer trap sites and as a result has higher structural and optical quality than the other spots.

To obtain vibrational structural information on the $MAPbI_3$ films to correlate with our micro PL measurements, resonance Raman spectra were collected from the same microspots where the PL was measured. Figure 1e shows the Raman spectra corresponding to the spots **A**, **B**, and **C** in which several peaks at 82, 105, 120, and 150 cm^{-1} were identified through Lorentzian fit functions (summarized in Table S2). In the spectra, the 150 cm^{-1} mode is clearly visible in spots **A** and **B**, but it is not found in spot **C**. However, all of the spots have the three common peaks at 82, 105, and 120 cm^{-1}, and their relative Raman intensity ratios are similar. These latter peaks correspond to Raman modes found in pure PbI_2 whose stretching vibrations are found at 76, 97, and 110 cm^{-1}, suggesting that the probed spots have similar octahedral Pb–I bonds.[49] However, PbI_2 does not have Raman modes at around 150 cm^{-1}. Therefore, the Raman modes at 150 cm^{-1} are uniquely related to the presence of MA^+ ions in the $MAPbI_3$ structure.

These unique MA Raman modes have been discussed in theoretical and experimental studies regarding structural deformations induced by degradation or a phase transition.[6,41,44] However, here we found that this previously overlooked MA Raman peak at 150 cm^{-1} has different intensities in the different microspots. The brightest spot **A** has the largest 150 cm^{-1} Raman peak, the second brightest **B** spot has a comparatively smaller 150 cm^{-1} mode intensity, and the dark **C** spot does not exhibit this feature. Figure 2a and b present contour plots of PL intensities and the corresponding intensity contour of the normalized 150 cm^{-1} Raman peaks, respectively. Figure 2c shows Raman spectra measured at the bright spots, which display the characteristic 150 cm^{-1} Raman peak. The contour comparison shows that every strong 150 cm^{-1} peak corresponds to an intense PL peak although there are a few PL peaks related with weaker Raman intensity. Figure S4 presents a scatter plot of the PL intensity against the Raman intensity and correlations with different thresholds between PL intensities and Raman intensities at 150 cm^{-1}. This observation supports that the 150 cm^{-1} Raman mode is correlated with the higher PL microstructures.

To determine the character of the observed Raman modes, we performed DFT calculations to obtain vibrational displacements and frequencies for the tetragonal structure of $MAPbI_3$. At room temperature, the MA^+ ions are believed to rotate quasi-randomly, sampling different relative orientations with near-equal probability.[16] To account for the effects of different possible relative orientations of MA in our DFT calculations, we consider two tetragonal structures (T1 and T2) with different orientations for the MA dipoles: T1 has an antipolar in-plane arrangement, while T2 has a polar in-plane arrangement (Figure S5). Calculation details are provided in the Supporting Information. Computed lattice constants and vibrational frequencies are in good agreement with experiments and previous results.[50,51] The experimentally measured Raman peaks at 82, 105, and 120 cm^{-1} were assigned to our computed modes with frequencies 82.9, 110.6, and 129.7 cm^{-1} for T1 and 84.1, 110.0, and 128.1 cm^{-1} for T2, respectively (Figure 3). The displacement patterns of these vibrational modes consist predominantly of symmetric stretching motions of the Pb–I bonds. The 120 cm^{-1} mode involves additional small displacements of MA that arise from mixing of vibrations of the Pb–I and MA groups.[6,41] The details of the displacement patterns for each of the vibrational modes are illustrated in Figure 3. Interestingly, the 150 cm^{-1} Raman mode (assigned to the 158.5–159.5 cm^{-1} mode in our calculations and illustrated in Figure 3d) comprises a strong librational motion of MA that

DOI: 10.1021/acs.nanolett.7b00919
Nano Lett. 2017, 17, 4151–4157

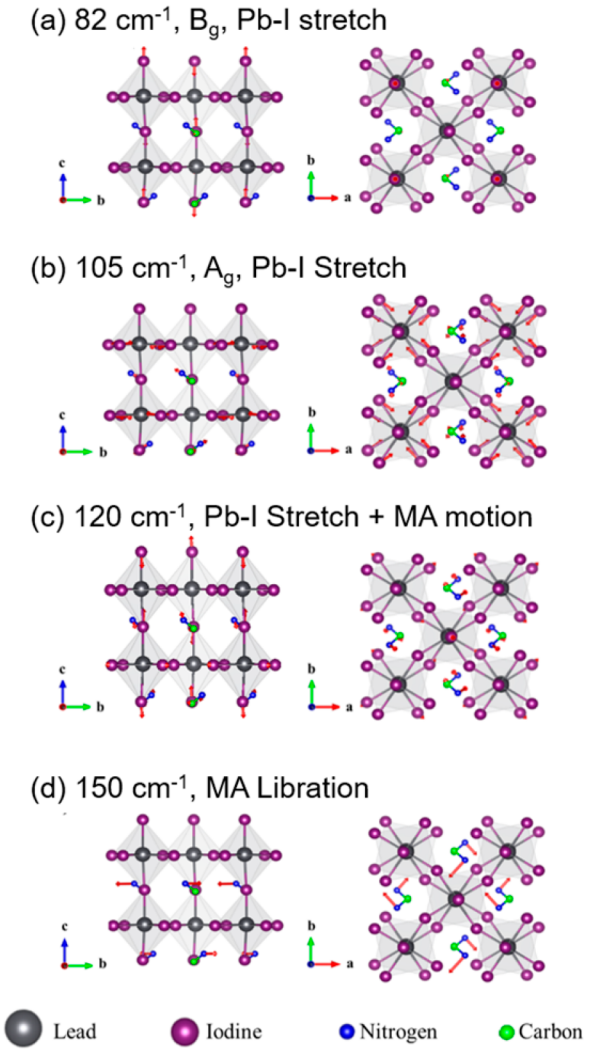

Figure 3. Calculated vibrational modes of $MAPbI_3$. Red arrows indicate the direction and amplitude of DFT calculated displacement patterns for the given Raman modes. (a) 82 cm^{-1} B_g mode involving alternating Pb−I stretching displacements along the *c*-axis, (b) 105 cm^{-1} A_g mode showing completely symmetric stretching motions of Pb−I in the *ab*-plane, (c) 120 cm^{-1} stretching motions of Pb−I + MA libration motion, and (d) 150 cm^{-1} libration motion of MA in the *ab*-plane.

takes place equatorially in the *ab*-plane with negligible displacements in the PbI_3 cages. This character distinguishes the 150 cm^{-1} mode from other low frequency lead iodide Raman modes. In addition, the replacement of MA with Cs shifts the computed phonon frequencies of tetragonal $CsPbI_3$ below 110 cm^{-1}, confirming the role of MA in the 150 cm^{-1} vibrational mode (see the Supporting Information).[52]

It has been emphasized that $MAPbI_3$ perovskite structures are stabilized by not only the suitable size of the intercalated MA and electrostatic interactions but also through the strong HB between the MA^+ ions and the PbI_6^{4-} octahedra.[15,19] As shown in Figure 4, MA^+ displays one long and two short hydrogen bonds, connecting each N−H moiety to either an equatorial (I_1) or axial (I_2 and I_3) iodine atom. The averaged distances are found to be 3.05, 2.65, and 2.63 Å for T1 and 3.02, 2.65, and 2.65 Å for T2, for equatorial and axial iodine atoms, indicating that HB interactions are significantly stronger to the axial iodine atoms. This HB-induced asymmetry may

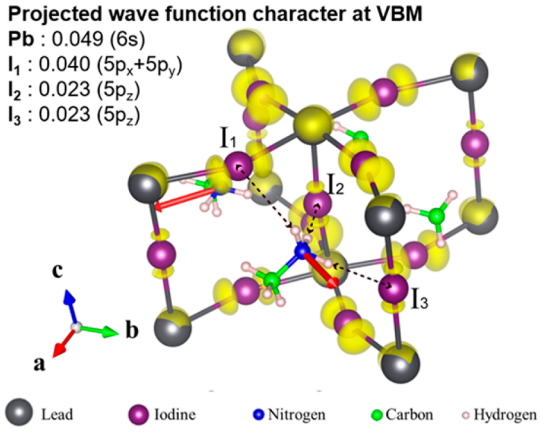

Figure 4. Perspective view of the 150 cm^{-1} librational motion of MA along with an isosurface plot of the square of the wave function for the valence band maximum (VBM) of the T1 structure. Red arrows indicate the direction of displacements for the eigenvector mode. Hydrogen-bonding (HB) between the H atoms of MA and I atoms is weaker with the equatorial I (I_1) and stronger with the axial I atoms (I_2 and I_3).

play a significant role in electrostatically inducing the distorted octahedral structure, according to Lee et al.'s recent work, where strong HB interactions are found in tilted octahedral perovskite systems.[19] In addition, the asymmetric HB interactions have a differential effect on the σ^* antibonding molecular orbital (MO) for the axial and equatorial iodines. Figure 4 presents an isosurface plot of the square of the wave function for the VBM of T1, where the electrons are seen to be delocalized through a σ^* antibonding MO consisting primarily of Pb 6s and I 5p orbitals.[53] Our DFT study shows that due to the directional nature of the HB interaction with MA, the projected wave function character for the p_x and p_y orbitals of iodine, $|\langle\psi|Y_{nlm}\rangle|^2$, with $l = 1$ for the VBM, are found to be significantly greater on the equatorial iodines (0.040) than on the two axial iodines (0.023) in arbitrary units [Figure 4; ψ and Y_{nlm} are the wave function and spherical harmonics with quantum number (nlm), respectively]. These results indicate that electrons on iodines at the VBM are not homogeneously delocalized due to the tilted lower-symmetry framework caused by the asymmetric HB interactions.

Based on the discussions above, the librational motion of MA in the *ab* plane will modulate the HB strength with the axial iodines. Thus, Raman spectra should be highly sensitive to changes in HB caused by structural perturbations or defects that in turn affect excited-state dynamics and PL efficiencies. The formation and location of the HB in the Pb−I framework during $MAPbI_3$ crystallization are critical for the stabilization of its structure and properties. Improper formation of this HB, e.g., through deficient location or orientation of the MA^+ ions, will result in distorted MA librational modes that in turn will be difficult to measure due to lower intensity or inhomogeneous broadening, as seen in the case of spot **C**. In contrast, a higher-quality homogeneous microstructure, such as in spot **A**, will exhibit brighter PL and a more pronounced Raman feature at 150 cm^{-1}.

To explore in more detail how the MA librational motion interacts with the structure of $MAPbI_3$, we have performed DFT calculations on two additional optimized $MAPbI_3$ structures ($-T_{MA}$ and $+T_{MA}$) based on the T1 structure by adding small rotations (~10°) of MA along the forward and

DOI: 10.1021/acs.nanolett.7b00919
Nano Lett. 2017, 17, 4151−4157

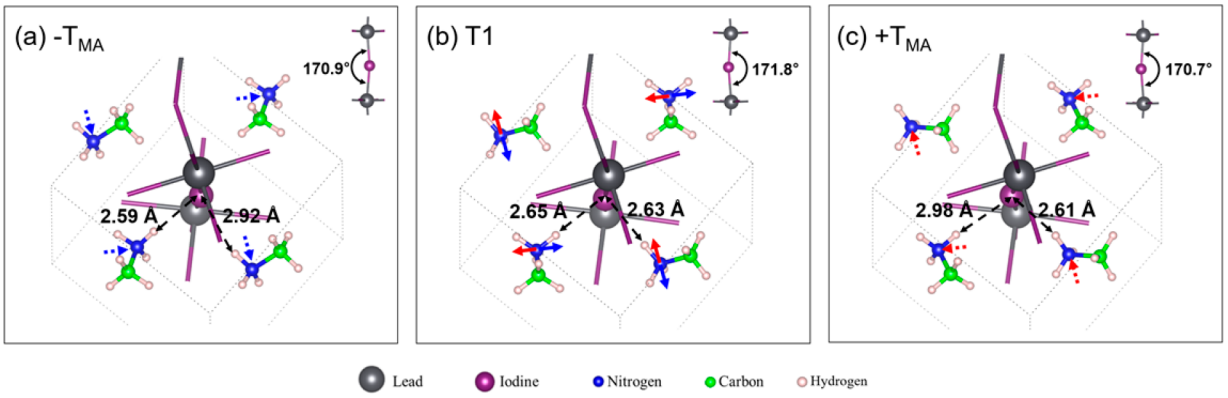

Figure 5. Optimized $MAPbI_3$ for (a) $-T_{MA}$, (b) T1, and (c) $+T_{MA}$ structure. Red and blue arrows indicate forward (+) and reverse (−) directions of the MA librational motion, respectively. NH···I distances and the acute Pb−I−Pb bond angles independent on orientation are shown for each structure.

reverse direction of the 150 cm^{-1} Raman mode and relaxing the Pb−I framework (Figure 5). The major new features for $-T_{MA}$ and $+T_{MA}$ are the NH···I distances are calculated to be 2.59/2.92 Å and 2.98/2.61 Å as a result of the 150 cm^{-1} librational motion. The axial iodines of $\pm T_{MA}$ are bent in opposite directions by the MA librational motion as a result of the strong HB interaction with the MA hydrogens. These results clearly indicate that the MA librational motion can influence the structural properties of the Pb−I framework through HB interaction changes, although the MA orbital levels do not electronically take part in the VBM and CBM levels.[53]

MA librational motion is an important factor for the highly enhanced carrier lifetimes of $MAPbI_3$.[23,26] According to previous work, ultrafast (sub-picosecond) dynamic molecular reorientation of fluctuating MA molecules can lead to a "dynamic Rashba splitting" and the consequent dynamical change of the band structure leading to a longer excited-state lifetime.[31,32] In contrast to "static" indirect band gap materials, perovskite with the dynamic Rashba splitting may still have a significant PL intensity. This is because the MA librational motions at 150 cm^{-1} is energetically on the order of kT. This small energy gap (18 meV) allows a dynamic or transient transition to a direct band gap luminescent excited-state and back at room temperature.[23] Moreover, the lifetime of this PL will be extended because the indirect band gap population has weaker radiative coupling.[54]

Our calculated valence and conduction band structures for $\pm T_{MA}$ and T1 including spin−orbit coupling show significant Rashba splitting of the CBM in the T1 structure and that this splitting is sensitive to the distortion amplitude along the MA librational coordinate (Figure S6). Thus, the dynamic librational motion of MA in the Pb−I framework is significant in three ways: (1) our Raman and PL results clearly show that the enhanced 150 cm^{-1} Raman mode is correlated with the higher PL intensity, (2) the MA librational motion effectively modulates the strength of the HBs by changing the dipole orientation of the MA^+ ions as well as the NH···I distances, and (3) the libration induces transient structural distortions and tilts of the Pb−I framework along with dynamical changes of the Rashba splitting of the band structures. This also suggests that the MA librational motion can be regarded as a CB relaxation coordinate to the indirect band gap state, since the intensity of a resonance Raman mode directly indicates the magnitude and direction of excited-state atomic relaxation.[55−57]

Our results are in good agreement with other recent studies on MA dynamics in the Pb−I framework. The librational motion at 150 cm^{-1} (temporal period of 150 cm^{-1} = 225 fs) is on the same time scale as the recently studied subpicosecond ~300 fs "wobbling-motion" of MA which was introduced as the first step for the full ferroelectric transition,[18] and the ~140 fs lifetime of the collective reorientational motion of MA responsible for polaron generation.[24,58] In addition, recent photocurrent microscopy measurements have found different photocurrent efficiencies of $MAPbI_{3-x}Cl_x$ microstructures due to MA's rotational motion.[48] Thus, the rotation dynamics of MA affect excited-state dynamics and alter PL efficiency as well as PV efficiency, reflecting the structural significance of the 150 cm^{-1} Raman mode. In contrast, microstructures lacking librational vibrations at 150 cm^{-1}, like site **C**, have a relatively low PL quantum yield.

In summary, we performed micro-PL and -Raman spectroscopies to probe the optoelectronic structure−function relationships in $MAPbI_3$. Different frequencies and intensities are observed for the MA librational Raman mode in microstructures of $MAPbI_3$ that are correlated to PL intensities. The dominant Raman peak at 150 cm^{-1} is found in microstructures exhibiting higher PL intensities. This mode is theoretically determined to be sensitive to the strength of the HB interactions between the hydrogens in MA and the iodines in the Pb−I framework which depend on the local structure. In addition, the dynamic distortion of the framework induced by the MA motion in the excited-state seems likely to influence the Rashba splitting resulting in a longer excited-state lifetime together with strong PL intensities. Thus, our results, supported with DFT calculations, indicate that the HB interactions and dynamics of MA in the Pb−I framework are mechanistically relevant for perovskite materials with high PL efficiency. Detailed studies on the excited state atomic dynamics of MA in inorganic perovskite $MAPbI_3$ are now needed to learn more about the possible role of dynamic structural distortions in producing efficient PV materials.

■ ASSOCIATED CONTENT

Supporting Information

The Supporting Information is available free of charge on the ACS Publications website at DOI: 10.1021/acs.nanolett.7b00919.

Experimental methods, fitting results for PL and Raman spectroscopy, and DFT results are summarized in

DOI: 10.1021/acs.nanolett.7b00919
Nano Lett. 2017, 17, 4151−4157

supporting tables. XRD spectrum, PL spectra of macro- and microscopic samples, a scatter plot of the PL intensity against the 150 cm^{-1} Raman intensity and correlations with different thresholds between PL intensities and Raman intensities at 150 cm^{-1}, calculated configurations of T1 and T2, and band structures for $-T_{MA}$, T1, and $+T_{MA}$ (PDF)

AUTHOR INFORMATION

Corresponding Author

*E-mail: ramathies@berkeley.edu.

ORCID

Myeongkee Park: 0000-0002-5307-2564

Peidong Yang: 0000-0003-4799-1684

Present Address

N.K.: Department of Chemistry, University of Cambridge, Lensfield Road, Cambridge CB2 1EW, United Kingdom.

Author Contributions

M.P. and N.K. contributed equally to this work. M.P., N.K., and R.A.M. conceived the project; S.E.R-L. undertook the DFT calculation with contribution from J.B.N.; M.P. and N.K. collected the PL and Raman data with contribution from P.Y. and analyzed the data with S.E.R.-L.; M.L. prepared the sample and collected additional data; M.P., N.K., S.E.R.-L., and R.A.M. wrote the manuscript with contributions and advice from all others.

Funding

M.P. was supported by the Mathies Royalty Fund. N.K. was supported by US Department of Energy, Office of Basic Energy Sciences (contract no. DE-AC02-05CH11231). Theory and computation were supported by the US Department of Energy, Office of Science, Office of Basic Energy Sciences (Theory FWP) Materials Sciences and Engineering Division (DE-AC02-05CH11231). Work at the Molecular Foundry was supported by the Office of Science, Office of Basic Energy Sciences, of the US Department of Energy under Contract No. DE-AC02-05CH11231. This work was supported by the Physical Chemistry of Inorganic Nanostructures Program, KC3103, Office of Basic Energy Sciences of the United States Department of Energy under Contract No. DE-AC02-05CH11231

Notes

The authors declare no competing financial interest.

ACKNOWLEDGMENTS

M.P. thanks Letian Dou for valuable discussions. S.E.R.-L. thanks Linn Leppert and Jung-Hoon Lee for valuable discussions. M.L. thanks Suzhou Industrial Park for the fellowship support. N.K. acknowledges the Royal Society Newton International Fellowship.

ABBREVIATIONS

$MAPbI_3$, methylammonium lead iodide; PL, photoluminescence; HB, hydrogen bonding; CBM, conduction band minimum; VBM, valence band maximum; OD, optical density; DFT, density-functional theory

REFERENCES

(1) Jung, H. S.; Park, N. G. *Small* **2015**, *11*, 10−25.
(2) Niu, G.; Guo, X.; Wang, L. *J. Mater. Chem. A* **2015**, *3*, 8970−8980.
(3) Sum, T. C.; Mathews, N. *Energy Environ. Sci.* **2014**, *7*, 2518−2534.
(4) Yang, W. S.; Noh, J. H.; Jeon, N. J.; Kim, Y. C.; Ryu, S.; Seo, J.; Seok, S. I. *Science* **2015**, *348*, 1234−1237.
(5) Chen, Q.; De Marco, N.; Yang, Y.; Song, T.-B.; Chen, C.-C.; Zhao, H.; Hong, Z.; Zhou, H.; Yang, Y. *Nano Today* **2015**, *10*, 355−396.
(6) Brivio, F.; Frost, J. M.; Skelton, J. M.; Jackson, A. J.; Weber, O. J.; Weller, M. T.; Goni, A. R.; Leguy, A.; Barnes, P. R.; Walsh, A. *Phys. Rev. B: Condens. Matter Mater. Phys.* **2015**, *92*, 144308.
(7) Dou, L.; Wong, A. B.; Yu, Y.; Lai, M.; Kornienko, N.; Eaton, S. W.; Fu, A.; Bischak, C. G.; Ma, J.; Ding, T.; Ginsberg, N. S.; Wang, L.-W.; Alivisatos, A. P.; Yang, P. *Science* **2015**, *349*, 1518−1521.
(8) Stranks, S. D.; Eperon, G. E.; Grancini, G.; Menelaou, C.; Alcocer, M. J. P.; Leijtens, T.; Herz, L. M.; Petrozza, A.; Snaith, H. J. *Science* **2013**, *342*, 341−344.
(9) Sun, S. J.; Fang, Y. N.; Kieslich, G.; White, T. J.; Cheetham, A. K. *J. Mater. Chem. A* **2015**, *3*, 18450−18455.
(10) Kieslich, G.; Sun, S. J.; Cheetham, A. K. *Chem. Sci.* **2015**, *6*, 3430−3433.
(11) Shi, D.; Adinolfi, V.; Comin, R.; Yuan, M.; Alarousu, E.; Buin, A.; Chen, Y.; Hoogland, S.; Rothenberger, A.; Katsiev, K.; Losovyj, Y.; Zhang, X.; Dowben, P. A.; Mohammed, O. F.; Sargent, E. H.; Bakr, O. M. *Science* **2015**, *347*, 519−522.
(12) Ning, Z. J.; Gong, X. W.; Comin, R.; Walters, G.; Fan, F. J.; Voznyy, O.; Yassitepe, E.; Buin, A.; Hoogland, S.; Sargent, E. H. *Nature* **2015**, *523*, 324−328.
(13) Solis-Ibarra, D.; Smith, I. C.; Karunadasa, H. I. *Chem. Sci.* **2015**, *6*, 4054−4059.
(14) Lee, J. H.; Bristowe, N. C.; Bristowe, P. D.; Cheetham, A. K. *Chem. Commun.* **2015**, *51*, 6434−6437.
(15) Leguy, A. M. A.; Frost, J. M.; McMahon, A. P.; Sakai, V. G.; Kochelmann, W.; Law, C. H.; Li, X. E.; Foglia, F.; Walsh, A.; O'Regan, B. C.; Nelson, J.; Cabral, J. T.; Barnes, P. R. F. *Nat. Commun.* **2015**, *6*, 7124−7133.
(16) Mattoni, A.; Filippetti, A.; Saba, M. I.; Delugas, P. *J. Phys. Chem. C* **2015**, *119*, 17421−17428.
(17) Peng, W.; Miao, X.; Adinolfi, V.; Alarousu, E.; El Tall, O.; Emwas, A.-H.; Zhao, C.; Walters, G.; Liu, J.; Ouellette, O.; Pan, J.; Murali, B.; Sargent, E. H.; Mohammed, O. F.; Bakr, O. M. *Angew. Chem., Int. Ed.* **2016**, *55*, 10686−10690.
(18) Bakulin, A. A.; Selig, O.; Bakker, H. J.; Rezus, Y. L. A.; Müller, C.; Glaser, T.; Lovrincic, R.; Sun, Z.; Chen, Z.; Walsh, A.; Frost, J. M.; Jansen, T. L. C. *J. Phys. Chem. Lett.* **2015**, *6*, 3663−3669.
(19) Lee, J. H.; Bristowe, N. C.; Lee, J. H.; Lee, S. H.; Bristowe, P. D.; Cheetham, A. K.; Jang, H. M. *Chem. Mater.* **2016**, *28*, 4259−4266.
(20) Gélvez-Rueda, M. C.; Cao, D. H.; Patwardhan, S.; Renaud, N.; Stoumpos, C. C.; Schatz, G. C.; Hupp, J. T.; Farha, O. K.; Savenije, T. J.; Kanatzidis, M. G.; Grozema, F. C. *J. Phys. Chem. C* **2016**, *120*, 16577−16585.
(21) Li, X.; Dar, M. I.; Yi, C.; Luo, J.; Tschumi, M.; Zakeeruddin, S. M.; Nazeeruddin, M. K.; Han, H.; Graetzel, M. *Nat. Chem.* **2015**, *7*, 703−711.
(22) Yin, W.-J.; Shi, T.; Yan, Y. *Appl. Phys. Lett.* **2014**, *104*, 063903.
(23) Motta, C.; El-Mellouhi, F.; Kais, S.; Tabet, N.; Alharbi, F.; Sanvito, S. *Nat. Commun.* **2015**, *6*, 7026.
(24) Zhu, H. M.; Miyata, K.; Fu, Y. P.; Wang, J.; Joshi, P. P.; Niesner, D.; Williams, K. W.; Jin, S.; Zhu, X. Y. *Science* **2016**, *353*, 1409−1413.
(25) Neukirch, A. J.; Nie, W.; Blancon, J.-C.; Appavoo, K.; Tsai, H.; Sfeir, M. Y.; Katan, C.; Pedesseau, L.; Even, J.; Crochet, J. J.; Gupta, G.; Mohite, A. D.; Tretiak, S. *Nano Lett.* **2016**, *16*, 3809−3816.
(26) Frost, J. M.; Butler, K. T.; Brivio, F.; Hendon, C. H.; van Schilfgaarde, M.; Walsh, A. *Nano Lett.* **2014**, *14*, 2584−2590.
(27) Brivio, F.; Walker, A. B.; Walsh, A. *APL Mater.* **2013**, *1*, 042111.
(28) Fan, Z.; Sun, K.; Wang, J. *J. Mater. Chem. A* **2015**, *3*, 18809−18828.
(29) Gottesman, R.; Haltzi, E.; Gouda, L.; Tirosh, S.; Bouhadana, Y.; Zaban, A.; Mosconi, E.; De Angelis, F. *J. Phys. Chem. Lett.* **2014**, *5*, 2662−2669.

DOI: 10.1021/acs.nanolett.7b00919
Nano Lett. 2017, 17, 4151−4157

(30) Frost, J. M.; Walsh, A. *Acc. Chem. Res.* **2016**, *49*, 528−535.
(31) Etienne, T.; Mosconi, E.; De Angelis, F. *J. Phys. Chem. Lett.* **2016**, *7*, 1638−1645.
(32) Zheng, F.; Tan, L. Z.; Liu, S.; Rappe, A. M. *Nano Lett.* **2015**, *15*, 7794−7800.
(33) Slavney, A. H.; Smaha, R. W.; Smith, I. C.; Jaffe, A.; Umeyama, D.; Karunadasa, H. I. *Inorg. Chem.* **2017**, *56*, 46.
(34) Smith, I. C.; Hoke, E. T.; Solis-Ibarra, D.; McGehee, M. D.; Karunadasa, H. I. *Angew. Chem., Int. Ed.* **2014**, *53*, 11232−11235.
(35) Mosconi, E.; Azpiroz, J. M.; De Angelis, F. *Chem. Mater.* **2015**, *27*, 4885−4892.
(36) Tong, C.-J.; Geng, W.; Tang, Z.-K.; Yam, C.-Y.; Fan, X.-L.; Liu, J.; Lau, W.-M.; Liu, L.-M. *J. Phys. Chem. Lett.* **2015**, *6*, 3289−3295.
(37) Han, Y.; Meyer, S.; Dkhissi, Y.; Weber, K.; Pringle, J. M.; Bach, U.; Spiccia, L.; Cheng, Y.-B. *J. Mater. Chem. A* **2015**, *3*, 8139−8147.
(38) Yang, J.; Siempelkamp, B. D.; Liu, D.; Kelly, T. L. *ACS Nano* **2015**, *9*, 1955−1963.
(39) Ledinsky, M.; Loeper, P.; Niesen, B.; Holovsky, J.; Moon, S.-J.; Yum, J.-H.; De Wolf, S.; Fejfar, A.; Ballif, C. *J. Phys. Chem. Lett.* **2015**, *6*, 401−406.
(40) Pérez-Osorio, M. A.; Milot, R. L.; Filip, M. R.; Patel, J. B.; Herz, L. M.; Johnston, M. B.; Giustino, F. *J. Phys. Chem. C* **2015**, *119*, 25703−25718.
(41) Park, B.-w.; Jain, S. M.; Zhang, X.; Hagfeldt, A.; Boschloo, G.; Edvinsson, T. *ACS Nano* **2015**, *9*, 2088−2101.
(42) Gonzalez-Pedro, V.; Juarez-Perez, E. J.; Arsyad, W.-S.; Barea, E. M.; Fabregat-Santiago, F.; Mora-Sero, I.; Bisquert, J. *Nano Lett.* **2014**, *14*, 888−893.
(43) Grancini, G.; Marras, S.; Prato, M.; Giannini, C.; Quarti, C.; De Angelis, F.; De Bastiani, M.; Eperon, G. E.; Snaith, H. J.; Manna, L.; Petrozza, A. *J. Phys. Chem. Lett.* **2014**, *5*, 3836−3842.
(44) Gottesman, R.; Gouda, L.; Kalanoor, B. S.; Haltzi, E.; Tirosh, S.; Rosh-Hodesh, E.; Tischler, Y.; Zaban, A.; Quarti, C.; Mosconi, E.; De Angelis, F. *J. Phys. Chem. Lett.* **2015**, *6*, 2332−2338.
(45) deQuilettes, D. W.; Vorpahl, S. M.; Stranks, S. D.; Nagaoka, H.; Eperon, G. E.; Ziffer, M. E.; Snaith, H. J.; Ginger, D. S. *Science* **2015**, *348*, 683−686.
(46) Christians, J. A.; Miranda Herrera, P. A.; Kamat, P. V. *J. Am. Chem. Soc.* **2015**, *137*, 1530−1538.
(47) Leguy, A. M. A.; Hu, Y.; Campoy-Quiles, M.; Alonso, M. I.; Weber, O. J.; Azarhoosh, P.; van Schilfgaarde, M.; Weller, M. T.; Bein, T.; Nelson, J.; Docampo, P.; Barnes, P. R. F. *Chem. Mater.* **2015**, *27*, 3397−3407.
(48) Leblebici, S. Y.; Leppert, L.; Li, Y.; Reyes-Lillo, S. E.; Wickenburg, S.; Wong, E.; Lee, J.; Melli, M.; Ziegler, D.; Angell, D. K.; Ogletree, D. F.; Ashby; Paul, D.; Toma, F. M.; Neaton, J. B.; Sharp, I. D.; Weber-Bargioni, A. *Nat. Energy* **2016**, *1*, 16093.
(49) Capozzi, V.; Fontana, A.; Fontana, M. P.; Mariotto, G.; Montagna, M.; Viliani, G. *Nuovo Cimento B* **1977**, *39*, 556−568.
(50) Quarti, C.; Mosconi, E.; De Angelis, F. *Chem. Mater.* **2014**, *26*, 6557−6569.
(51) Quarti, C.; Mosconi, E.; Ball, J. M.; D'Innocenzo, V.; Tao, C.; Pathak, S.; Snaith, H. J.; Petrozza, A.; De Angelis, F. *Energy Environ. Sci.* **2016**, *9*, 155−163.
(52) Calistru, D. M.; Mihut, L.; Lefrant, S.; Baltog, I. *J. Appl. Phys.* **1997**, *82*, 5391−5395.
(53) Yin, W.-J.; Shi, T.; Yan, Y. *Adv. Mater.* **2014**, *26*, 4653−4658.
(54) Kirchartz, T.; Rau, U. *J. Phys. Chem. Lett.* **2017**, *8*, 1265−1271.
(55) Lee, S. Y.; Heller, E. J. *J. Chem. Phys.* **1979**, *71*, 4777−4788.
(56) Myers, A. B.; Mathies, R. A.; Spiro, T. G. *Biological Applications Of Raman Spectroscopy, Vol. 2 Resonance Raman Spectra Of Polyenes And Aromatics* **1987**, *2*, 1−58.
(57) Lin, C.; Gong, K.; Kelley, D. F.; Kelley, A. M. *J. Phys. Chem. C* **2015**, *119*, 7491−7498.
(58) Zhu, X. Y.; Podzorov, V. *J. Phys. Chem. Lett.* **2015**, *6*, 4758−4761.

DOI: 10.1021/acs.nanolett.7b00919
Nano Lett. 2017, 17, 4151−4157